nature geoscience

ARTICLES

https://doi.org/10.1038/s41561-020-0587-0

Southern Ocean carbon sink enhanced by sea-ice feedbacks at the Antarctic Cold Reversal

C. J. Fogwill[1,2]✉, C. S. M. Turney[2,3,4], L. Menviel[2,5], A. Baker[2,3], M. E. Weber[6], B. Ellis[7], Z. A. Thomas[2,3,4], N. R. Golledge[8,9], D. Etheridge[10], M. Rubino[1,10,11], D. P. Thornton[10], T. D. van Ommen[12,13], A. D. Moy[12,13], M. A. J. Curran[12,13], S. Davies[14], M. I. Bird[15,16], N. C. Munksgaard[15,17], C. M. Rootes[18], H. Millman[1,5], J. Vohra[2], A. Rivera[19,20], A. Mackintosh[21], J. Pike[22], I. R. Hall[22], E. A. Bagshaw[22], E. Rainsley[1], C. Bronk-Ramsey[23], M. Montenari[1], A. G. Cage[1], M. R. P. Harris[1], R. Jones[24,28], A. Power[25], J. Love[25], J. Young[26], L. S. Weyrich[3,26] and A. Cooper[27]

The Southern Ocean occupies 14% of the Earth's surface and plays a fundamental role in the global carbon cycle and climate. It provides a direct connection to the deep ocean carbon reservoir through biogeochemical processes that include surface primary productivity, remineralization at depth and the upwelling of carbon-rich water masses. However, the role of these different processes in modulating past and future air–sea carbon flux remains poorly understood. A key period in this regard is the Antarctic Cold Reversal (ACR, 14.6–12.7 kyr BP), when mid- to high-latitude Southern Hemisphere cooling coincided with a sustained plateau in the global deglacial increase in atmospheric CO_2. Here we reconstruct high-latitude Southern Ocean surface productivity from marine-derived aerosols captured in a highly resolved horizontal ice core. Our multiproxy reconstruction reveals a sustained signal of enhanced marine productivity across the ACR. Transient climate modelling indicates this period coincided with maximum seasonal variability in sea-ice extent, implying that sea-ice biological feedbacks enhanced CO_2 sequestration and created a substantial regional marine carbon sink, which contributed to the plateau in CO_2 during the ACR. Our results highlight the role Antarctic sea ice plays in controlling global CO_2, and demonstrate the need to incorporate such feedbacks into climate–carbon models.

The Last Glacial Transition (LGT; 18,000–11,000 yr ago or 18–11 kyr BP) experienced rapid and sustained changes in atmospheric CO_2 (increasing from approximately 190 ppm to around 270 ppm; Fig. 1), providing the opportunity to gain valuable insights into climate–carbon dynamics[1]. Detailed analysis of the stable isotopic composition of atmospheric carbon dioxide ($\delta^{13}C$-CO_2)[1,2] from Antarctic ice cores suggests terrestrial carbon may have played a substantial role in rapid CO_2 rises, but variability across the LGT may reflect a combination of sources, sinks and feedbacks. Parallel changes in Antarctic temperature and atmospheric CO_2 have been interpreted as the Southern Ocean playing a key role in the global carbon budget[3–5], but detailed mechanisms remain unresolved. Several physical and biological mechanisms have been invoked to explain these observations, including: changes in the strength and/or latitudinal migration of the mid-latitude jet stream and prevailing surface westerly airflow influencing Southern Ocean overturning[4,6–8], variations in iron (dust) fertilization of subantarctic phytoplankton impacting the biological carbon pump efficiency[9–11], sea-ice controlling CO_2 exchange[12,13] and carbon drawdown[14], and the potential impacts of a warming ocean on CO_2 exchange[1].

[1]School of Geography, Geology and the Environment, Keele University, Keele, UK. [2]Palaeontology, Geobiology and Earth Archives Research Centre, School of Biological, Earth and Environmental Sciences, UNSW Sydney, Sydney, New South Wales, Australia. [3]ARC Centre of Excellence in Australian Biodiversity and Heritage, School of Biological, Earth and Environmental Sciences, UNSW Sydney, Sydney, New South Wales, Australia. [4]Chronos 14Carbon-Cycle Facility, UNSW Sydney, Sydney, New South Wales, Australia. [5]Climate Change Research Centre, School of Biological, Earth and Environmental Sciences, UNSW Sydney, Sydney, New South Wales, Australia. [6]Department of Geochemistry and Petrology, Institute of Geosciences, University of Bonn, Bonn, Germany. [7]Research School of Earth Sciences, Australian National University, Canberra, Australian Capital Territory, Australia. [8]Antarctic Research Centre, Victoria University of Wellington, Wellington, New Zealand. [9]GNS Science, Lower Hutt, New Zealand. [10]CSIRO Oceans and Atmosphere, Aspendale, Victoria, Australia. [11]Dipartimento di Matematica e Fisica, Università della Campania "Luigi Vanvitelli", Caserta, Italy. [12]Australian Antarctic Division, Department of Agriculture, Water and the Environment, Kingston, Tasmania, Australia. [13]Antarctic Climate and Ecosystems Cooperative Research Centre, University of Tasmania, Hobart, Tasmania, Australia. [14]Department of Geography, Swansea University, Swansea, UK. [15]Centre for Tropical Environmental and Sustainability Science, College of ScienceTechnology and Engineering, James Cook University, Cairns, Queensland, Australia. [16]ARC Centre of Excellence in Australian Biodiversity and Heritage, James Cook University, Cairns, Queensland, Australia. [17]Research Institute for the Environment and Livelihoods, Charles Darwin University, Darwin, Northern Territory, Australia. [18]Department of Geography, University of Sheffield, Sheffield, UK. [19]Instituto de Conservación, Biodiversidad y Territorio, Universidad Austral de Chile, Valdivia, Chile. [20]Departamento de Geografia, Universidad de Chile, Santiago, Chile. [21]School of Earth, Atmosphere and Environment, Monash University, Melbourne, Victoria, Australia. [22]School of Earth and Ocean Sciences, Cardiff University, Cardiff, UK. [23]Research Laboratory for Archaeology and the History of Art, University of Oxford, Oxford, UK. [24]School of Geography, Exeter University, Exeter, UK. [25]Bioeconomy Centre, Exeter University, Exeter, UK. [26]Australian Centre for Ancient DNA, University of Adelaide, Adelaide, South Australia, Australia. [27]South Australian Museum, Adelaide, South Australia, Australia. [28]Deceased: R. Jones. ✉e-mail: c.j.fogwill@keele.ac.uk

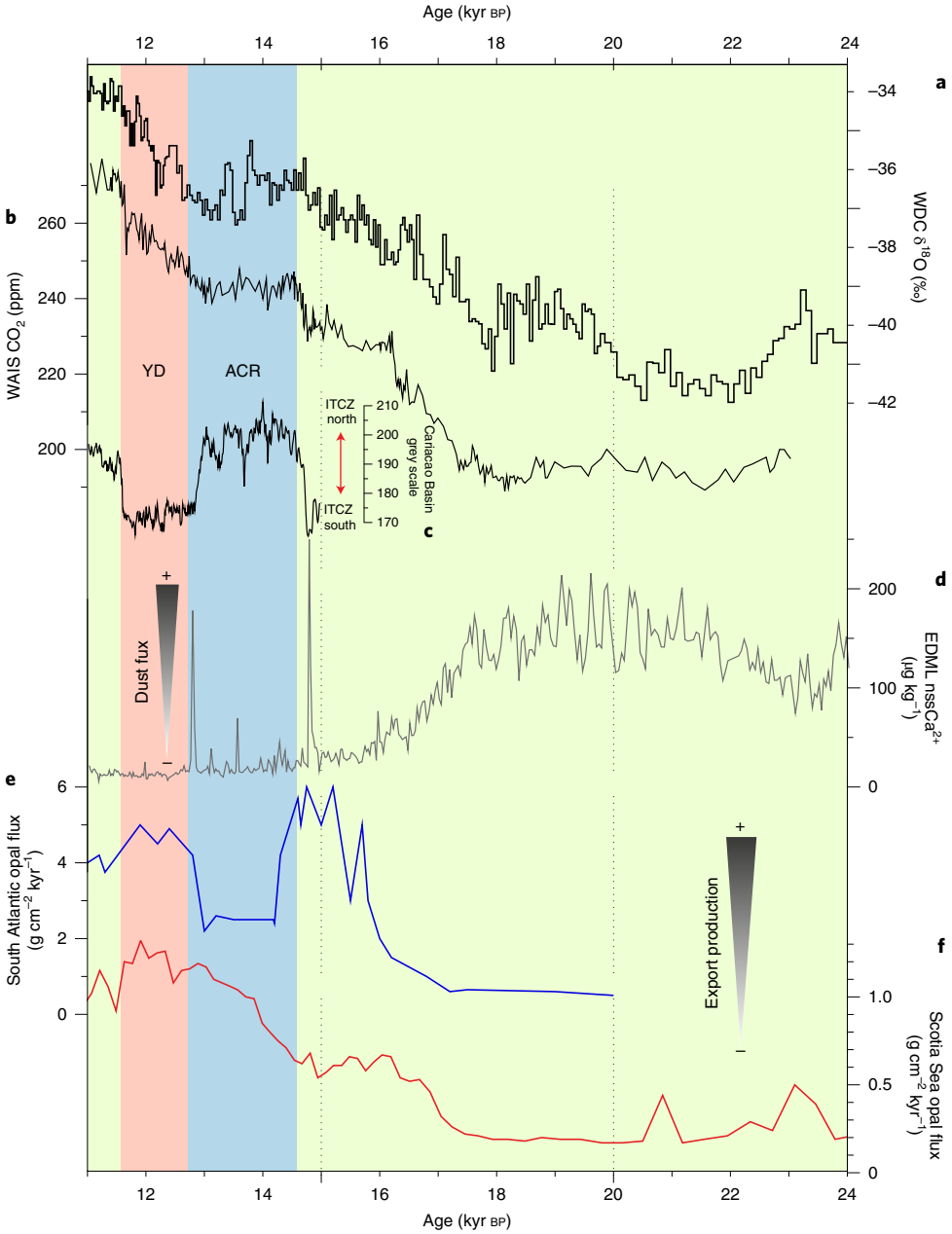

Fig. 1 | Intercomparison of Antarctic ice core with marine proxy records from independent referenced studies. a, WAIS Divide core (WDC[51]) $\delta^{18}O$ isotopic record. **b**, CO_2 concentration from WDC (WD_{2014} chronology)[17]. **c**, Cariaco Basin grey scale (measure of latitudinal changes in the trade winds related to the Intertropical Convergence Zone (ITCZ)[48]). **d**, Non-sea-salt Ca^{2+} ($nssCa^{2+}$) from EDML[52]. **e**, South Atlantic opal flux from TN057-13 (blue)[4]. **f**, Scotia Sea opal flux core MD07-3134 (red)[21]. Vertical boxes indicate the periods defined by the ACR (blue) and the Younger Dryas (YD) chronozone (pink; 11.7–12.7 kyr BP).

The role of the Southern Ocean as a source or sink of atmospheric carbon during the LGT remains highly contested, with the above processes not fully accounting for the changes in CO_2 recorded over this period[9], implying that one or more mechanisms are currently not captured in our understanding[15,16].

A striking feature of the LGT record is a 1,900-yr-long plateau in CO_2 concentration, when the ongoing rise in CO_2 paused at a near-constant 240 ppm during the Antarctic Cold Reversal (ACR)[17], a period characterized by surface cooling across the mid- to high latitudes of the Southern Hemisphere[18–20]. The ACR was coincident with sustained warming across the Northern Hemisphere (the North Atlantic Bølling–Allerød interstadial)[9,17] and abrupt global sea-level rise[21,22], as well as major disruptions to atmospheric and ocean circulation[8,22] and the carbon cycle (Fig. 1)[9,10,23]. While the global sequence of events during the ACR is reasonably well known[19], a clear understanding of the drivers and impacts of contrasting polar climate changes on global CO_2 trends has proved elusive, owing to the challenges in precisely aligning ice and marine records across this period[9]; this is compounded by the lack of well-resolved, high-accumulation marine sedimentary records from the high-latitude Southern Ocean.

One crucial record in this regard comes from marine sediment core TN057-13 (~53 °S 5 °E)[4,9] (Fig. 2), which suggests the ACR was characterized by reduced carbon sequestration in the mid- to high

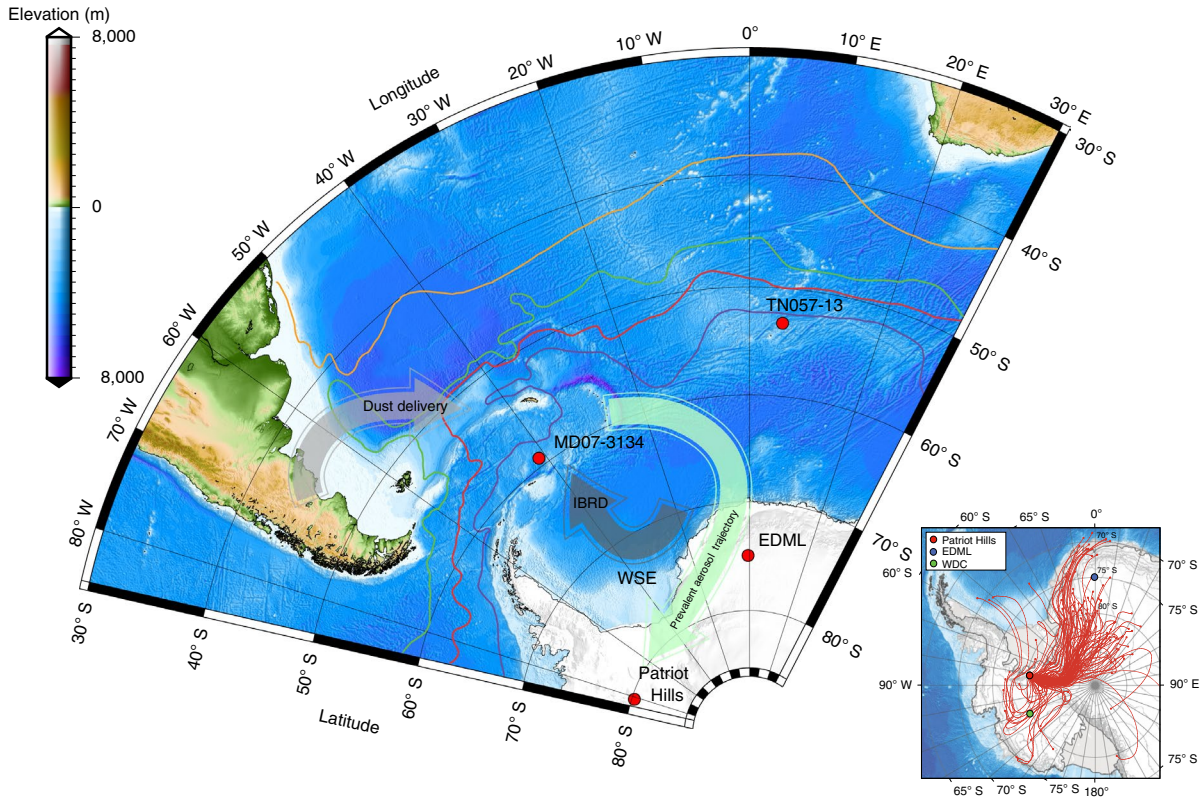

Fig. 2 | The South Atlantic sector of the Southern Ocean with the locations of the Patriot Hills in the Ellsworth Mountains, the EDML ice core and marine cores MD07-313421 and TN057-134. Positions of the southern limb of the Antarctic Circumpolar Current (purple line), the Polar Front (red), Subantarctic Front (green) and the Subtropical Front (yellow)[53]. The grey arrow denotes the primary route of iceberg-rafted debris (IBRD) in the Weddell Sea Embayment (WSE), and the green arrow depicts the prevalent aersol trajectory to the Patriot Hills site. Inset, monthly grouped 72 h atmospheric back-trajectories for the Patriot Hills (November 2009), from the NOAA HySPLIT[54], with WDC and EDML[52] ice cores. South Pole stereographic basemap produced in Generic Mapping Tools v5.4.5 (ref. [55]) with the NOAA ETOPO1 Ice Surface dataset.

latitudes (measured by decreased biological productivity or export production[4,5]; Fig. 1e). This event was possibly the result of enhanced stratification, which decreased the vertical supply of nutrients across the high-nutrient, low-chlorophyll (HNLC) sectors of the Southern Ocean during cooling[4]. However, such a hypothesis is difficult to test in the absence of a network of well-resolved records of productivity from the high latitudes of the Southern Ocean.

Southern Ocean productivity polewards of TN057-13 has been previously recorded in the Scotia Sea from marine core MD07-3134 (~59 °S 42 °W; Figs. 1f and 2 and Supplementary Information)[21]. In common with core TN057-13, this sequence is exceptionally well resolved (with sedimentation rates of 20–200 cm kyr^{-1} according to ref. [21]) and, given the location, records changes south of the Polar Front, even during glacial terminations[24]. After accounting for sediment focusing with ^{230}Th normalization (Supplementary Information)[25], MD07-3134 opal burial rates provide estimated changes in biological productivity (export production) (Fig. 1f). This marine sequence records increased export production in the high-latitude Southern Ocean from 17 kyr BP, in line with that shown to the north in core TN057-13; however, subsequently, export production in the high-latitude Southern Ocean (MD07-3134) continued to increase through the ACR, in antiphase to the trend recorded further north (TN057-13)[4] (Figs. 1 and 2). These divergent trends suggest that different driver(s) of marine biological activity may have operated across the high latitudes, contributing to the sustained ACR CO_2 plateau.

In the absence of a network of highly resolved marine records from the high-latitude Southern Ocean (that are normalized through ^{230}Th)[24], we present a new reconstruction of high-latitude surface ocean productivity from aerosol-derived marine biomarkers captured in a highly resolved horizontal ice core from the Weddell Sea, Antarctica[22], which records regional-scale environmental processes operating across the South Atlantic sector of the Southern Ocean during the LGT (Fig. 2)[22,26].

The Patriot Hills blue ice record

A new 'horizontal' ice core record was developed from the exposed blue ice area (BIA) at the Patriot Hills in Horseshoe Valley in the Ellsworth Mountains (Fig. 2)[22], where ancient ice has been drawn up to the surface of the ice sheet. With a well-constrained chronology, uninterrupted sequence of ice through the LGT (Fig. 3; and Methods) and contemporary precipitation and aerosol delivery from the South Atlantic sector of the Southern Ocean (Fig. 2 and Supplementary Information)[27], the Patriot Hills is ideally placed to record environmental changes across the high-latitude South Atlantic. The record provides unrestricted volumes of ice of known age, offering a unique opportunity to develop innovative multiproxy biomarker reconstructions[22,28]. In contrast to many other BIAs, the site has not been mixed through ice flow, providing a coherent stratigraphic succession across the LGT (Fig. 3, Methods and Supplementary Information)[22,29].

Identifying marine biomarkers in ancient ice

To examine regional environmental responses through the LGT, fluorescent organic matter (fOM) analysis and liquid chromatography organic carbon detection (LC-OCD)[30] were undertaken across

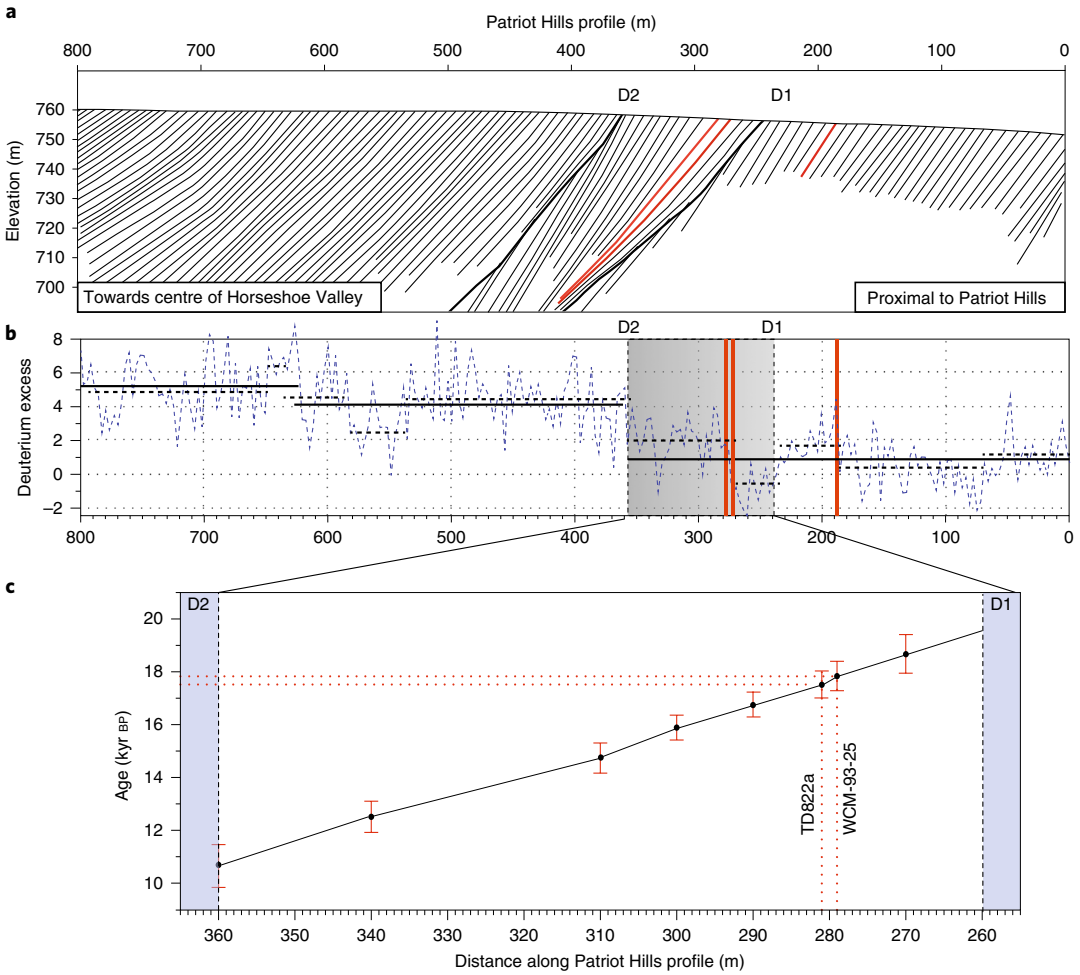

Fig. 3 | Stratigraphic and chronological details of the Patriot Hill BIA. a, Schematic stratigraphic succession from ground-penetrating radar across the Patriot Hills BIA, indicating ice accumulation punctuated by two periods of erosion (D1 and D2; thick black lines), and the position of known tephras (red lines)[22]. **b**, Deuterium excess across profile; solid horizontal black lines denote potential regime shifts at 99% confidence, and dashed black lines denote potential regime shifts at 95% confidence[38]. **c**, Age–depth model between D1 ~21 kyr BP and D2 ~10 kyr BP with volcanic 'tephra' horizons (TD822a and WCM-93-25) marked with error bars from absolute (tephras) or trace gas analysis (see the Supplementary Information and ref. [22]).

the Patriot Hills record, to identify biomarker signals and quantify changes in dissolved organic carbon (DOC) before and after the ACR (Fig. 4, Methods and Supplementary Information)[30]. Detailed analysis (using an Aqualog) of fOM emission spectra from samples taken at depth identified two protein-like components in ice across the profile, TRYLIS and TYLIS: tryptophan and tyrosine-like substances[31] (Methods and Supplementary Information). While there are limited studies of such biomarkers in ancient Antarctic ice[32], past work has demonstrated that a strong TRYLIS microbial signal is found in contemporary Antarctic snow and ice, derived predominantly from precipitation and aerosols from the Southern Ocean[33–35]. Previous work on the West Antarctic Ice Sheet (WAIS) Divide ice core using similar fOM approaches, as well as epifluorescence microscopy and flow cytometry, has identified chlorophyll and tryptophan in ancient ice, demonstrating that these are primarily derived from marine aerosol sources, with only a minor component being geomicrobial (in situ) in origin[34,35] (Methods and Supplementary Information). These studies have also identified interannual variability in the fOM signal, concluding that in situ secondary production or post-depositional alteration of fOM in ice are unlikely to be factors in interpreting marine fOM signals from Antarctic ice cores (Methods and Supplementary Information)[34,35].

To examine the source of the fOM signal in the Patriot Hills BIA, and test our hypothesis of a marine origin[35], we applied imaging flow cytometry (IFC; ImageStream) and scanning electron microscopy (SEM) to the Patriot Hills samples to identify microscopic populations within the ice (Fig. 4, Methods and Supplementary Information). IFC on samples across the record reveals four distinct non-in situ microbial populations (Fig. 4c) based on the autofluorescence and morphology of particulates: nanoplankton[36], eukaryotic picoplankton[37], chitin[37] and crypto-tephra and/or wind-blown dust[22]. SEM analysis on unvortexed samples demonstrates that the eukaryotic picoplankton and the chitin populations are related (Fig. 4d). These marine populations are represented in all samples analysed throughout the profile, and while IFC is not quantitative, it provides valuable independent support for the fOM signal being marine in origin. Together, the fOM, LC-OCD and IFC analyses indicate that marine biomarkers are present throughout the profile, in agreement with other Antarctic ice-core studies[34,35].

Intercomparison of biomarkers from the Patriot Hills BIA

In comparing the records of fOM across the LGT, we observe a pronounced intensity peak related to autofluorescence of marine biomarkers across the ACR section of the Patriot Hills BIA (Figs. 4a and 5f).

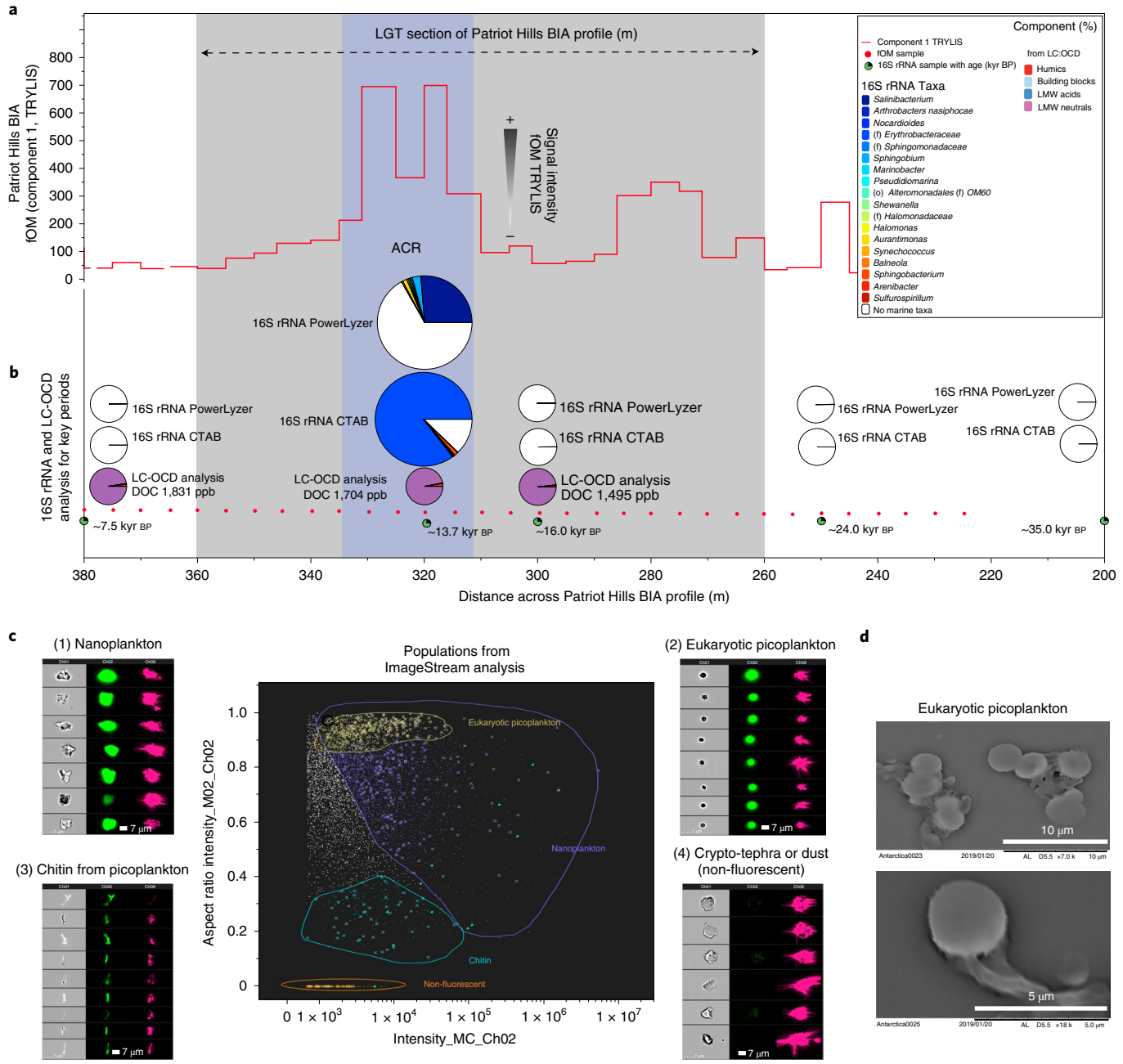

Fig. 4 | Marine biomarkers from Patriot Hills BIA. a, Five-m-resolved fOM intensity (arbitrary units). **b**, Percentage of marine taxa from 16S rRNA extractions by PowerLyzer (top), cetyl trimethylammonium bromide (CTAB) (middle) and LC-OCD component analysis (bottom) with DOC (ppb). LGT and ACR periods are highlighted in grey and blue, respectively. **c**, Marine populations from IFC (ImageStream) (sample 380 m): (1) nanoplankton, (2) eukaryotic picoplankton, (3) chitin and (4) non-fluorescent dust (left to right: brightfield (Ch01), autofluorescence (Ch02) and side scatter (Ch06)). Subpopulations were differentiated on the basis of the intensity of Ch02 (multiple channel mask (MC_Ch02), versus aspect ratio (individual channel mask (M02_ Ch02) (centre plot). **d**, SEM of picoeukaryotes with chitin (tails) at original magnification, ×7,000 (top) and ×16,000 (bottom).

This change in fOM signal could reflect marked changes in precipitation source over the LGT; however, we discount this through regime shift analysis[38] on the deuterium excess profile, which reveals no significant variability across the ACR or the LGT, at either 99% or 95% confidence, indicating that the precipitation source remained constant over the LGT (Fig. 3b). This implies that the intensity of the fOM signal reflects an increase in the autofluorescent marine biomarkers in the precipitation and aerosol source regions, associated with nanoplankton, picoplankton and picoeukaryotes as identified through IFC. We focus on the variation in the TRYLIS fOM component, which represents 83.33% of the variance in fOM signal (Methods and Supplementary Information). The TRYLIS component is highly variable across the BIA record, but has a sustained high concentration across the period defined by the ACR (Figs. 4 and 5). This pattern is mirrored in samples taken from a parallel transect from the Patriot Hills BIA, demonstrating the robustness of the fOM signal (Extended Data Fig. 1).

To further investigate the detail of the marine biomarker signals, large-volume ice samples were taken across key transitions of the Patriot Hills BIA to extract ancient bacterial DNA

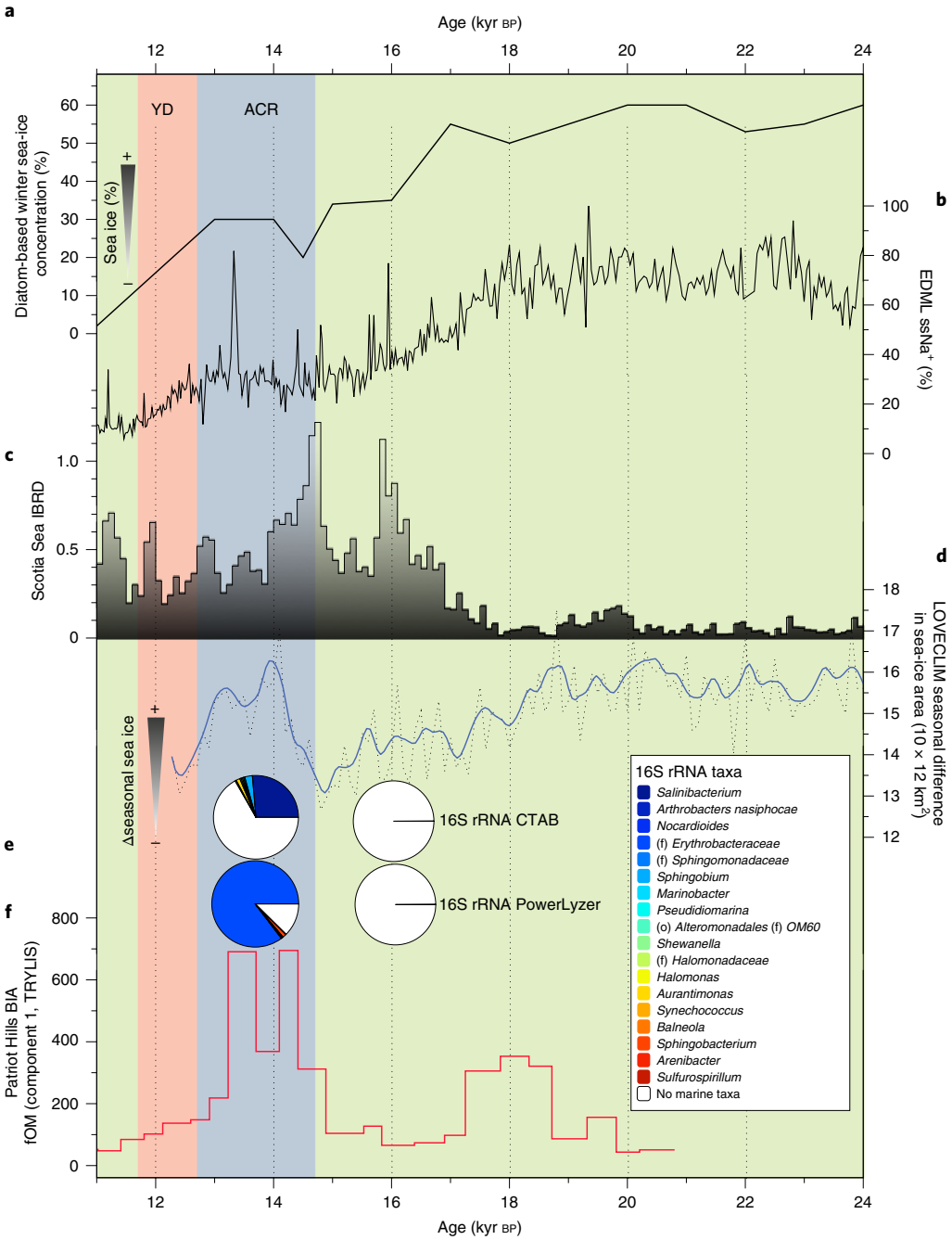

Fig. 5 | Regional climate proxy and model intercomparisons with the Patriot Hills record. a, Diatom transfer function-based winter sea-ice concentration[41]. **b**, Sea salt (ssNa$^+$) from EDML[52]. **c**, Iceberg-rafted debris (IBRD) from MD07-3134[21] (normalized 100 yr, relative to the Holocene). **d**, Modelled seasonal difference in Antarctic sea-ice area (LOVECLIM[42]). **e**, Percentage marine microorganisms from 16S rRNA CTAB extraction (top) and PowerLyzer (bottom). **f**, fOM concentration (component 1; TRYLIS). Vertical boxes indicate the ACR (blue) and YD chronozones (11.7–12.7 kyr BP).

in situ by directly melting and filtering ice from specific time horizons—maximizing the signal and minimizing contamination (Fig. 4b, Methods and Supplementary Information)—allowing the identification of picoplankton, picoeukaryotes and nanoplankton at taxon level. The 16S ribosomal RNA indexing reveals that a marked ecological switch—characterized by the appearance of an exceptionally diverse range of halotolerant microorganisms commonly found in seawater—was observed through the ACR, coincident with the increase in the fOM TRYLIS signal (Fig. 4b). Specifically, we found that the marine-associated taxa *Salinibacterium*, (f) *Erythrobacteraceae*, *Rhodobacteraceae*, *Marinobacter* and *Pseudidiomarina* are statistically associated with the ACR period ($P < 0.038$). The increase in species diversity (predominantly marine taxa) compared with that observed during either the mid-Holocene or Last Glacial Maximum is marked (Figs. 4 and 5). While the source of this signal could have been from brine pools associated with sea-ice build-up, the signal likely reflects an enhanced diversity and productivity from an open marine, or marginal sea-ice zone, an interpretation that agrees with the WAIS Divide ice-core analysis[34,35].

With four independent approaches (LC-OCD, IFC analysis, fOM and DNA) providing a record of marine biological productivity in the high-latitude South Atlantic sector of the Southern Ocean, our results strongly suggest that the ACR was a period of enhanced marine biological productivity and diversity. With the enhanced picoplankton and picoeukaryotes signals derived from the surface precipitation and aerosol source waters of the HNLC Southern Ocean during the ACR, we suggest that there was sustained strengthening of the biological pump, similar to the effects of contemporary iron fertilization experiments[16], a finding consistent with the enhanced export production recorded in marine sediments from the Scotia Sea (Fig. 1f)[21].

Comparison between marine and terrestrial records

To reconcile the apparent conflict between the increase in marine productivity across the ACR recorded in marine cores from the Scotia Sea (MD07-3134) and the Patriot Hills BIA with the decrease reported further north in the South Atlantic (TN057-13)[4,9] (Fig. 1), we compare our record of marine biomarkers (fOM) captured in the Patriot Hills ice with potential drivers of Southern Ocean productivity: IBRD (a proxy for Antarctic iceberg discharge)[21], sea salt sodium ($ssNa^+$) from the European Project for Ice Coring in Antarctica (EPICA) Dronning Maud Land (EDML) ice core (a proxy for sea-ice extent)[39] and proxy sea-ice reconstructions[40,41]. We further compare these records with published independent transient modelling experiments using LOVECLIM, which include freshwater hosing in the Ross and Weddell seas[42] (Fig. 5 and Supplementary Information). During the LGT, these comparisons indicate weak relationships between inferred marine biological productivity, sea-ice expansion, atmospheric CO_2 variability and the peak in marine-derived biomarkers (fOM) between ~24 and ~14.6 kyr BP, agreeing with previous studies (Fig. 5)[43]. This contrasts with the period defined by the ACR, where we observe a strong relationship between marine fOM in the Patriot Hills BIA, increased production of biogenic opal in the Scotia Sea, and the extended atmospheric CO_2 plateau (Figs. 1 and 5). Given that this increase in marine productivity seen in the Scotia Sea during the ACR is not apparent in mid-latitude marine records (Fig. 2)[4,9], we focus on possible high-latitude drivers of CO_2 exchange: iron fertilization from enhanced IBRD flux[44], a reduction in Antarctic Bottom Water (AABW) formation due to enhanced freshwater flux[45–47] and sea-ice feedbacks[40].

IBRD contains high concentrations of bioavailable iron, making iceberg melt a potential source for increased primary productivity and carbon sequestration through fertilization across the HNLC regions of the high-latitude Southern Ocean[44]. However, despite evidence of potential enhanced iron fertilization of the Southern Ocean through increased delivery of IBRD at around 20–19 kyr BP and 17–16 kyr BP[21], there does not appear to be a strong biological response in the Patriot Hills fOM or Scotia Sea opal flux records (Figs. 2 and 5), suggesting that enhanced IRBD influx did not lead to increased high-latitude marine export production. Another possibility is ice-sheet drawdown across the Weddell Sea Embayment[21,22], with associated meltwater influx that may have triggered stratification and substantial circulation changes across the broader Southern Ocean, magnified by associated shifts in the intensity and/or location of surface westerly airflow[4,9,22,48]; this is supported by independent ice-sheet and Earth-system modelling experiments[21,42]. However, the disparity in the opal flux records between marine cores from the mid-latitude South Atlantic[4] and Scotia Sea argues that the enhanced ACR export production was focused on the high-latitude South Atlantic across the Scotia Sea (Fig. 1).

An alternative mechanism involves sea-ice feedbacks, which have been implicated in amplifying climate and ice sheet feedbacks across the ACR[19,46]. Recent studies of full glacial conditions suggest that reduced surface–deep ocean exchange and enhanced

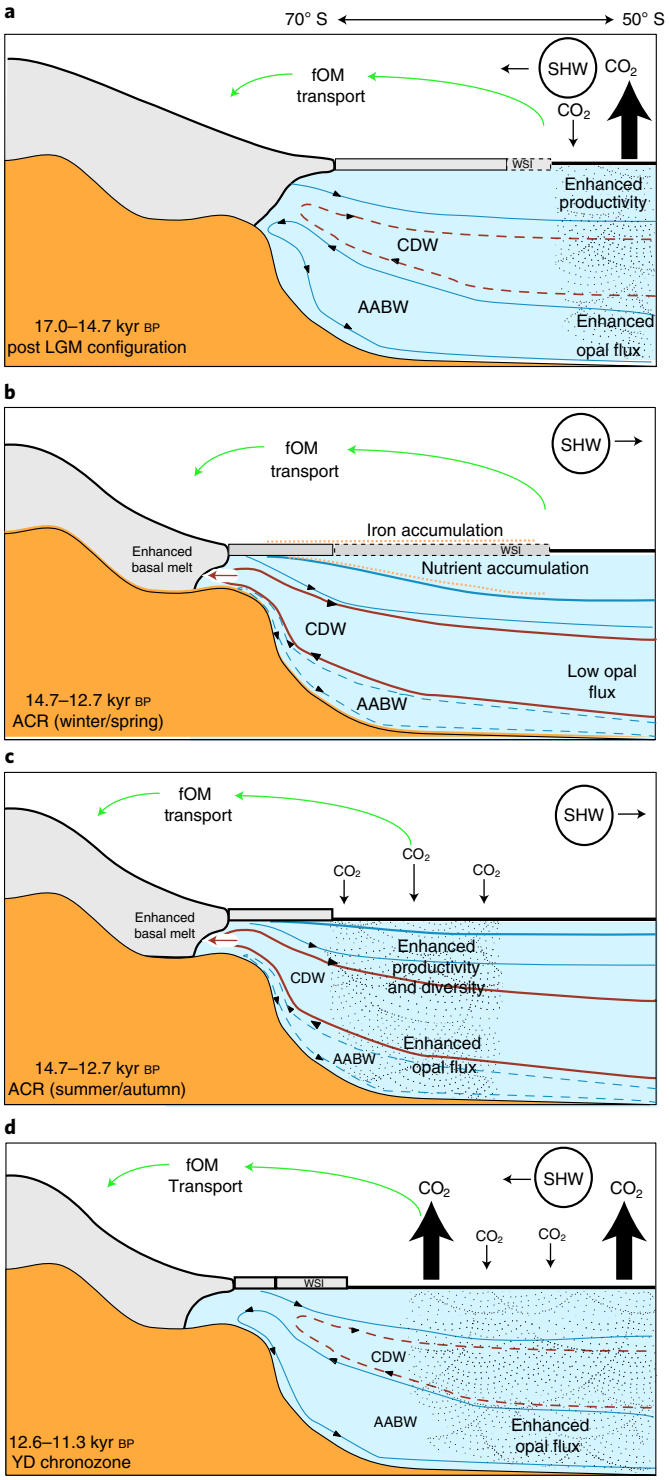

Fig. 6 | Schematic depicting events across mid- to high-latitude Southern Ocean during the LGT. a, Post-Last Glacial Maximum (LGM). Displacement of the Southern Hemisphere westerlies (SHW) enhances overturning of mid-latitude Southern Ocean between ~17 and 14.7 kyr BP evidenced by opal flux[4]. **b**, ACR. Enhanced intrusion of Circumpolar Deepwater (CDW) and winter sea-ice (WSI) expansion (winter/spring winter). Increased stratification, mixed layer deepening and reduction in AABW[40]. **c**, ACR (summer/autumn) during which the WSI breakup enhances CO_2 drawdown at high latitudes. **d**, YD chronozone, with reinvigorated mid-latitude overturning and degassing of old CO_2 enhancing opal flux.

micronutrient consumption by phytoplankton in the Southern Ocean may have lowered atmospheric CO_2 (refs. [40,43]). During the austral winter, sea-ice expansion allowed the mixed layer to deepen, 'refuelling' the surface ocean with micronutrients from the deep ocean reservoir and enhancing near-surface productivity and export production during the breakup of sea ice in the subsequent summer. This was probably amplified by the addition of iron from sea-ice melt and breakup in the post-glacial HNLC ocean, and possibly also by seasonal temperature changes and $CaCO_3$ dissolution[13]. Proxy records and the LOVECLIM transient Earth-system modelling[42] suggest that the highest seasonal variability in sea-ice extent across the LGT took place during the ACR (with greatest extent during winter and spring) (Fig. 5), implying that sea-ice feedbacks were amplified across this period (Fig. 6). These conditions contrast markedly with the periods immediately prior to (Fig. 6a) and following (Fig. 6d) the ACR, when the seasonal sea-ice zone was relatively less variable (Fig. 5), the high-latitude Southern Ocean less stratified[21,42,46], and the locations of the Intertropical Convergence Zone and mid-latitude Southern Hemisphere westerlies were relatively south (Fig. 2). Set against a backdrop of a warming ocean during the LGT, these conditions probably created ideal conditions for enhanced Southern Ocean productivity in the high-latitude Southern Ocean, especially in sectors of the South Atlantic such as the Weddell and Scotia seas.

Comparison between the continuous Scotia Sea opal flux record[21] and the Patriot Hills BIA fOM record indicates that the high-latitude signal of enhanced surface marine primary productivity was related to marked seasonal sea-ice variability during the ACR, a period characterized by a sustained atmospheric CO_2 plateau[9,17,23]. During the ACR, most marine records across the mid-latitudes suggest that the biological pump in the Southern Ocean weakened, in apparent contradiction to the plateau in atmospheric CO_2 at that time (Fig. 1). Our results indicate that, despite low dust input (Fig. 1) and surface cooling across subantarctic waters during the ACR, marked variability in sea-ice extent resulted in increased seasonal surface productivity in the HNLC waters of the high-latitude South Atlantic sector of the Southern Ocean, compared with periods before and following this event (Fig. 5). We suggest that increased seasonal marine primary productivity in fact enhanced the Southern Ocean organic carbon pump, increasing carbon drawdown and leading to enhanced export production (Fig. 6). Whilst other mechanisms may have played a part in the ACR CO_2 plateau—including iron fertilization, cool Southern Ocean surface temperatures and possibly reductions in the rate of AABW formation[8]—our observation that seasonal Southern Ocean sea-ice feedbacks in the South Atlantic sector of the high-latitude Southern Ocean may have contributed to a slowdown in the rate of CO_2 rise during the ACR has important implications for our understanding of the role of the Southern Ocean in global carbon dynamics. Our results imply that during periods of Southern Ocean sea-ice expansion, high variability in winter and summer sea-ice extent may result in enhanced carbon sequestration—as seen recently with marked sea-ice variability enhancing benthic carbon drawdown[14]—providing a negative feedback during periods of rising CO_2. This finding has ramifications for our understanding of contemporary ice–ocean–carbon feedbacks, and highlights the dynamic role that Antarctic sea ice plays in driving a negative feedback during periods of rising CO_2. This mechanism requires detailed modelling assessment with high-resolution tracer-enabled models that capture such processes[49], particularly given recent Antarctic sea-ice changes[50], which may impact the efficiency of the Southern Ocean as a carbon sink in the future[14].

Online content

Any methods, additional references, Nature Research reporting summaries, source data, extended data, supplementary information, acknowledgements, peer review information; details of author contributions and competing interests; and statements of data and code availability are available at https://doi.org/10.1038/s41561-020-0587-0.

Received: 3 September 2019; Accepted: 1 May 2020;
Published online: 22 June 2020

References

1. Bauska, T. K. et al. Carbon isotopes characterize rapid changes in atmospheric carbon dioxide during the last deglaciation. *Proc. Natl Acad. Sci. USA* **113**, 3465–3470 (2016).
2. Bauska, T. K. et al. Controls on millennial-scale atmospheric CO_2 variability during the last glacial period. *Geophys. Res. Lett.* **45**, 7731–7740 (2018).
3. Monnin, E. et al. Atmospheric CO_2 concentrations over the Last Glacial Termination. *Science* **291**, 112–114 (2001).
4. Anderson, R. F. et al. Wind-driven upwelling in the Southern Ocean and the deglacial rise in atmospheric CO_2. *Science* **323**, 1443–1448 (2009).
5. Gottschalk, J. et al. Biological and physical controls in the Southern Ocean on past millennial-scale atmospheric CO_2 changes. *Nat. Commun.* **7**, 11539 (2016).
6. Toggweiler, J. R., Russell, J. L. & Carson, S. R. Midlatitude westerlies, atmospheric CO_2, and climate change during the ice ages. *Paleoceanography* **21**, PA2005 (2006).
7. Marshall, J. & Speer, K. Closure of the meridional overturning circulation through Southern Ocean upwelling. *Nat. Geosci.* **5**, 171–180 (2012).
8. Huang, H., Gutjahr, M., Eisenhauer, A. & Kuhn, G. No detectable Weddell Sea Antarctic Bottom Water export during the Last and Penultimate Glacial Maximum. *Nat. Commun.* **11**, 14302 (2020).
9. Jaccard, S. L., Galbraith, E. D., Martínez-García, A. & Anderson, R. F. Covariation of deep Southern Ocean oxygenation and atmospheric CO_2 through the last ice age. *Nature* **530**, 207–210 (2016).
10. Martínez-García, A. et al. Iron fertilization of the Subantarctic ocean during the last ice age. *Science* **343**, 1347–1350 (2014).
11. Jaccard, S. L. et al. Two modes of change in Southern Ocean productivity over the past million years. *Science* **339**, 1419–1423 (2013).
12. Butterworth, B. J. & Miller, S. D. Air–sea exchange of carbon dioxide in the Southern Ocean and Antarctic marginal ice zone. *Geophys. Res. Lett.* **43**, 7223–7230 (2016).
13. Delille, B. et al. Southern Ocean CO_2 sink: the contribution of the sea ice. *J. Geophys. Res. Oceans* **119**, 6340–6355 (2014).
14. Barnes, D.K. Antarctic sea ice losses drive gains in benthic carbon drawdown. *Curr. Biol.* **25**, R789 (2015).
15. Boyd, P. W., Claustre, H., Levy, M., Siegel, D. A. & Weber, T. Multi-faceted particle pumps drive carbon sequestration in the ocean. *Nature* **568**, 327–335 (2019).
16. Boyd, P. W. et al. A mesoscale phytoplankton bloom in the polar Southern Ocean stimulated by iron fertilization. *Nature* **407**, 695–702 (2000).
17. Marcott, S. A. et al. Centennial-scale changes in the global carbon cycle during the last deglaciation. *Nature* **514**, 616–619 (2014).
18. Fogwill, C. J. & Kubik, P. W. A glacial stage spanning the Antarctic Cold Reversal in Torres del Paine (51°S), Chile, based on preliminary cosmogenic exposure ages. *Geogr. Ann. Ser. A* **87A**, 403–408 (2005).
19. Pedro, J. B. et al. The spatial extent and dynamics of the Antarctic Cold Reversal. *Nat. Geosci.* **9**, 51–55 (2015).
20. McGlone, M. S., Turney, C. S. M., Wilmshurst, J. M., Renwick, J. & Pahnke, K. Divergent trends in land and ocean temperature in the Southern Ocean over the past 18,000 years. *Nat. Geosci.* **3**, 622–626 (2010).
21. Weber, M. E. et al. Millennial-scale variability in Antarctic ice-sheet discharge during the last deglaciation. *Nature* **510**, 134–138 (2014).
22. Fogwill, C. et al. Antarctic ice sheet discharge driven by atmosphere–ocean feedbacks at the Last Glacial Termination. *Sci. Rep.* **7**, 39979 (2017).
23. Schmitt, J. et al. Carbon isotope constraints on the deglacial CO_2 rise from ice cores. *Science* **336**, 711–714 (2012).
24. Sprenk, D. et al. Southern Ocean bioproductivity during the last glacial cycle—new decadal-scale insight from the Scotia Sea. *Geol. Soc. Spec. Publ.* **381**, 245–261 (2013).
25. Meyer-Jacob, C. et al. Independent measurement of biogenic silica in sediments by FTIR spectroscopy and PLS regression. *J. Paleolimnol.* **52**, 245–255 (2014).
26. Turney, C. S. M. et al. Late Pleistocene and early Holocene change in the Weddell Sea: a new climate record from the Patriot Hills, Ellsworth Mountains, West Antarctica. *J. Quat. Sci.* **28**, 697–704 (2013).
27. Tetzner, D., Thomas, E. & Allen, C.A. Validation of ERA5 reanalysis data in the Southern Antarctic Peninsula—Ellsworth Land region, and its implications for ice core studies. *Geosciences* **9**, 289 (2019).
28. Turney, C. S. M. et al. Early Last Interglacial ocean warming drove substantial ice mass loss from Antarctica. *Proc. Natl Acad. Sci. USA* **117**, 3996–4006 (2020).

29. Winter, K. et al. Assessing the continuity of the blue ice climate record at Patriot Hills, Horseshoe Valley, West Antarctica. *Geophys. Res. Lett.* **43**, 2019–2026 (2016).
30. Huber, S. A., Balz, A., Abert, M. & Pronk, W. Characterisation of aquatic humic and non-humic matter with size-exclusion chromatography – organic carbon detection – organic nitrogen detection (LC-OCD-OND). *Water Res.* **45**, 879–885 (2011).
31. Jørgensen, L. et al. Global trends in the fluorescence characteristics and distribution of marine dissolved organic matter. *Mar. Chem.* **126**, 139–148 (2011).
32. D'Andrilli, J., Foreman, C. M., Sigl, M., Priscu, J. C. & McConnell, J. R. A 21,000 year record of organic matter quality in the WAIS Divide ice core. *Clim. Discuss.* **2016**, 1–15 (2016).
33. Smith, H. J. et al. Microbial formation of labile organic carbon in Antarctic glacial environments. *Nat. Geosci.* **10**, 356–359 (2017).
34. Rohde, R. A., Price, P. B., Bay, R. C. & Bramall, N. E. In situ microbial metabolism as a cause of gas anomalies in ice. *Proc. Natl Acad. Sci. USA* **105**, 8667–8672 (2008).
35. Price, P. & Bay, R. Marine bacteria in deep Arctic and Antarctic ice cores: a proxy for evolution in oceans over 300 million generations. *Biogeosciences* **9**, 3799–3815 (2012).
36. Moorthi, S., Caron, D., Gast, R. & Sanders, R. Mixotrophy: a widespread and important ecological strategy for planktonic and sea-ice nanoflagellates in the Ross Sea, Antarctica. *Aquat. Micro. Ecol.* **54**, 269–277 (2009).
37. Massana, R. Eukaryotic picoplankton in surface oceans. *Annu. Rev. Microbiol.* **65**, 91–110 (2011).
38. Rodionov, S.N. A sequential algorithm for testing climate regime shifts. *Geophys. Res. Lett.* **31**, L09204 (2004).
39. Wolff, E. W. et al. Southern Ocean sea-ice extent, productivity and iron flux over the past eight glacial cycles. *Nature* **440**, 491–496 (2006).
40. Abelmann, A. et al. The seasonal sea-ice zone in the glacial Southern Ocean as a carbon sink. *Nat. Commun.* **6**, 8136 (2015).
41. Esper, O. & Gersonde, R. New tools for the reconstruction of Pleistocene Antarctic sea ice. *Palaeogeogr. Palaeoclimatol. Palaeoecol.* **399**, 260–283 (2014).
42. Menviel, L., Timmermann, A., Elison Timm, O. & Mouchet, A. Deconstructing the Last Glacial Termination: the role of millennial and orbital-scale forcings. *Quat. Sci. Rev.* **30**, 1155–1172 (2011).
43. Collins, L. G., Pike, J., Allen, C. S. & Hodgson, D. A. High-resolution reconstruction of southwest Atlantic sea-ice and its role in the carbon cycle during marine isotope stages 3 and 2. *Paleoceanography* **27**, PA3217 (2012).
44. Duprat, L. P. A. M., Bigg, G. R. & Wilton, D. J. Enhanced Southern Ocean marine productivity due to fertilization by giant icebergs. *Nat. Geosci.* **9**, 219–221 (2016).
45. Fogwill, C. J., Phipps, S. J., Turney, C. S. M. & Golledge, N. R. Sensitivity of the Southern Ocean to enhanced regional Antarctic ice sheet meltwater input. *Earth Future* **3**, 317–329 (2015).
46. Golledge, N. R. et al. Antarctic contribution to meltwater pulse 1A from reduced Southern Ocean overturning. *Nat. Commun.* **5**, 6107 (2014).
47. Menviel, L., Timmermann, A., Timm, O. E. & Mouchet, A. Climate and biogeochemical response to a rapid melting of the West Antarctic Ice Sheet during interglacials and implications for future climate. *Paleoceanography* **25**, PA4231 (2010).
48. Hogg, A. Punctuated shutdown of Atlantic Meridional Overturning Circulation during the Greenland Stadial 1. *Sci. Rep.* **6**, 25902 (2016).
49. Menviel, L. et al. Southern Hemisphere westerlies as a driver of the early deglacial atmospheric CO_2 rise. *Nat. Commun.* **9**, 2503 (2018).
50. Parkinson, C. L. A 40-y record reveals gradual Antarctic sea ice increases followed by decreases at rates far exceeding the rates seen in the Arctic. *Proc. Natl Acad. Sci. USA* **116**, 14414–14423 (2019).
51. WAIS Divide Members Precise interpolar phasing of abrupt climate change during the last ice age. *Nature* **520**, 661–665 (2015).
52. Wolff, E. et al. Southern Ocean sea-ice extent, productivity and iron flux over the past eight glacial cycles. *Nature* **440**, 491–496 (2006).
53. Orsi, A. H., Whitworth, T. III & Nowlin, W. D. Jr. On the meridional extent and fronts of the Antarctic Circumpolar Current. *Deep Sea Res. Pt 1* **42**, 641–673 (1995).
54. Stein, A. et al. NOAA's HYSPLIT atmospheric transport and dispersion modeling system. *Bull. Am. Meteorol. Soc.* **96**, 2059–2077 (2015).
55. Wessel, P. et al. New, improved version of Generic Mapping Tools released. *Eos* **79**, 579–579 (1998).

Methods

Patriot Hills site description and chronology. The Patriot Hills BIA (Horseshoe Valley, Ellsworth Mountains; 80° 18′ S, 81° 21′ W) is a slow-flowing (<12 m yr^{-1}), locally sourced compound glacier system situated within an over-deepened catchment that is buttressed by, but ultimately coalesces with, the Institute Ice Stream close to the contemporary grounding line of the AIS[22]. The Patriot Hills BIA record is chronologically constrained by multiple greenhouse gas species (CO_2, CH_4 and N_2O) supported by geochemically identified volcanic (tephra) horizons (Fig. 3 and Supplementary Information); here we build on the chronology of previous studies[22] with increased sampling and the identification of more tephras, to provide tighter age control through the LGT. The age model demonstrates that this part of the BIA sequence spans from ~2.5 to 50 kyr BP, with two unconformities (discontinuities D1 and D2) that mark the build-up to (D1) and deglaciation from (D2) the last glacial cycle (Fig. 3)[22]. High-resolution ground-penetrating radar and detailed analysis of trace gases and volcanic tephra horizons[22] demonstrate that the conformable BIA layers (or 'isochrons') between these two unconformities span the period between ~11 to ~23 kyr BP (Fig. 3c). Thus, the horizontal ice core captures a unique highly resolved record of ice-sheet dynamics[22], in an area of exceptionally slow-moving ice[29], with no chronological breaks or unconformities across the LGT (Fig. 3a). Source areas for delivery of air masses to the Patriot Hills were investigated using the National Oceanic and Atmospheric Administration (NOAA) HySPLIT Lagrangian single-particle model[54]; interfacing and model parameterization were performed with the SplitR[56] and openair[57] packages for Rv3.6.0. Back-trajectories were forced with Global Data Assimilation System (GDAS) 1° meteorological data and generated at 6 h intervals, resulting in 112–124 trajectories per month (https://ready.arl.noaa.gov/HYSPLIT.php.). Climate reanalysis[27] and HySplit particle trajectory analysis demonstrate that contemporary snow and marine aerosol delivery at the site is associated with low-pressure systems that either have tracked across the Weddell Sea from the southern Atlantic Ocean, or relate to blocking by the Antarctic Peninsula (Fig. 2 and Supplementary Information)[26,27,58,59]. As such, the Patriot Hills BIA profile provides an opportunity to obtain large-volume ice samples of known ages for innovative multiproxy biomarker reconstruction, making it the ideal site to build up a record of environmental and ice-sheet change in this sector of Antarctica[22].

Sampling strategy. Sterile discrete samples were extracted from depth across the 800 m Patriot Hills BIA profile. For the fOM analysis, samples were taken across the full profile at ~5 m resolution (Fig. 4). To remove surface contaminants, the team first drilled down to 10 cm with a Jiffy ice drill to expose a fresh ice surface. Using a cleaned hand drill, an ~50-mm-long × ~25-mm-wide ice plug was extracted from the fresh surface and transferred into a gamma-sterilized 50 ml centrifuge tube that was sealed and double bagged. Samples were kept frozen until analysis, then thawed naturally in a refrigerator and analysed within 48 h before measurement against water and quinine sulphate blanks with no sample manipulation or pre-treatment on an Aqualog at UNSW IceLab (Supplementary Information).

fOM analysis. Detailed analysis of the fOM fluorescence emission spectra (using an Aqualog) from samples taken at depth identified two protein-like components in ice across the profile and in contemporary snow (Supplementary Information). Due to their excitation–emission wavelengths, we can unambiguously identify these fOM biomarker components as those widely reported in precipitation as TRYLIS and TYLIS: tryptophan and tyrosine-like substances[31], with TRYLIS making up over 83% of the total fOM signal in all samples analysed (Supplementary Information). While there are limited studies of such biomarkers in ancient Antarctic ice[32], past work has demonstrated that a strong TRYLIS microbial signal is found in Antarctic snow and ice derived from precipitation and aerosols from the marine environment[33–35]. Indeed, previous work on the WAIS Divide ice core using similar fOM approaches, epifloresence microscopy and flow cytometry has identified chlorophyll and tryptophan in ancient ice, and demonstrated that these are derived primarily from a Southern Ocean source with only a minor component being geomicrobial (in situ) in origin[34,35]. Furthermore, results from the WAIS Divide core also highlight that there is seasonal variability in the marine biomarker signal, with an estimated ~25% interannual variability at this inland site, and crucially that alteration of fOM in ice is unlikely to be a factor in interpreting the fOM signal in Antarctic ice-core studies[35].

To test for reproducibility of fOM, a selection of samples from a second parallel transect were run at UNSW IceLab in 2015, and subsequently at Keele IceLab on a different Aqualog in 2019 (Supplementary Information). Despite storage, the reproducibility between the transects and repeated analysis was robust and coherent (Supplementary Fig. S2).

Identification of marine biomarker populations in ancient ice. IFC analysis identified four populations in ancient and contemporary ice samples (Fig. 4 and Supplementary Information). The first population is composed of dark angular particles ~5–12 µm in length that have a high autofluorescence (Ch02) and a three-dimensional (3D) structure evidenced from a strong side scatter (Ch06) signal, which we classify as nanoplankton[36]. The second population is characterized by spheroidal forms ranging in diameter from ~2 to 5 µm that again have a high autofluorescence (Ch02) and a 3D structure evidenced from a strong side scatter (Ch06) signal, which we identify as eukaryotic picoplankton and picoeukaryotes[37]. The third population is characterized by elongate spicules or rods between 2 and 10 µm that have a high autofluorescence and a 3D structure evidenced from a side-scatter (Ch06) signal, which we identify as chitin, most likely related to the second population of eukaryotic picoplankton and picoeukaryotes[37], an interpretation confirmed through SEM (Fig. 4d). Finally, the fourth population comprises an inorganic fraction ranging from ~2 to 10 µm in length, characterized by a flaky flat structure and no autofluorescence, which we interpret as a mixture of crypto-tephra, and/or wind-blown dust[22]. Beyond these four populations, a few other events were recorded; these were identified as broken diatom frustules, characterized by a high autofluorescence and a side-scatter signal (Supplementary Information). These populations represent far-travelled 'aerosol'-transported marine detritus, which is not in situ derived or geomicrobial in origin[35]. Those with high autofluorescence (the eukaryotic picoplankton and picoeukaryotes, and chitin) clearly impact the fOM signal, but do not appear to substantially alter the DOC content of the sample; we suggest this reflects the fact that such planktonic forms represent an important dissolved inorganic carbon component of ancient ice from the Patriot Hills BIA record.

Of the populations identified through IFC, the nanoplankton, eukaryotic picoplankton and picoeukaryotes, and chitin populations made up ~46% of the total, with the non-fluorescent signal accounting for ~12%. Finally ~43% of the signal is unclassified at present and includes particulate less than 2 µm, which is difficult to identify due to its small size. However, ~20% of events within this fraction are characteristic of smaller picoeukaryotes, displaying similar properties to eukaryotic picoplankton identified in the >2 µm fraction[37]. The remaining particulate is comprised of 'elongate fluorescent rods' (likely chitin), and unclassified angular and round particulate matter again with high autofluorescence (Fig. 4 and Supplementary Information).

The fact that the picoplankton, picoeukaryotes, and chitin populations (>2 µm) were not recorded as one population in the IFC analysis is interesting, and likely reflects the process of the flow cytometry, where sheath fluids run through the machine at the same time as the sample—this focuses the sample into a steady stream, so that each 'event' can be analysed individually. This effect, or possibly vortexing before analysis, may have disaggregated the picoplankton and picoeukaryotes, separating the tails (chitin) from the spheroidal 'body' (Supplementary Information). To test this, SEM analysis was undertaken on samples that had not been previously unfrozen or analysed. SEM imaging demonstrated unambiguously that whole picoplankton and picoeukaryotes were present in the water samples from ancient ice, complete with chitin (Fig. 4d)[37].

Defining exotic aerosol-derived marine biomarker populations from in situ geomicrobial biomarkers. fOM analysis across the Patriot Hills BIA profile indicates that the TRYLIS intensity is a persistent signal, highly variable across centennial and millennial timescales. The relationship between in situ microbial (geomicrobial) production within a given medium and the resulting TRYLIS signal is complex, with microbes capable of producing TRYLIS fluctuations before population growth, and creating secondary fluorophores as a result of metabolic activity[60]. Given the absence of a relationship between any LC-OCD DOC components and the TRYLIS signal, and the IFC analysis identifying the microbial fraction as being predominantly planktonic in nature, we assert that secondary in situ metabolic activity is an unlikely explanation for the observed fluctuations in the TRYLIS fluorescence signal at Patriot Hills (Fig. 4b). It is possible, or even probable, that the presence and/or metabolic activity of microbial populations existing in situ accounts for a portion of the low 'baseline' fluorescence exhibited across many portions of the profile (Fig. 4a).

It is also possible that external 'fertilization' by the observed marine inputs could constitute a nutrient source for in situ production, thereby contributing to the TRYLIS intensity signal. However, IFC analysis demonstrates that the marked variability in the fOM signal across the profile relate to the presence of microscopic marine plankton, principally picoplankton and picoeukaryotes, but also with nanoplankton populations up to ~8 µm in size.

The distinct planktonic populations identified from IFC are particularly interesting, and as recorded in contemporary mesoscale experiments[16], picoplankton and picoeukaryotes form the basis of the pelagic community's response to iron fertilization in the high-latitude HLNC Southern Ocean, and are potentially key to CO_2 drawdown in the polar Southern Ocean[15]. The origin of these organisms can only be explained by precipitation or aerosol-derived marine detritus from the high-latitude Southern Ocean[26,34,35,58,59]. With the TRYLIS component also being identified in the WAIS Divide core[34] and in the fOM signal in contemporary snow cores from the Patriot Hills site that record the past decade (Methods and Supplementary Information), fOM provides a rapid, reproducible measure of high-latitude surface marine productivity that may be directly linked to export production in this sector of the Southern Ocean[16,34,35]. This premise is testable through comparison with analyses of marine sediments from sites such as the Scotia Sea (Fig. 1F).

Analysis of ancient DNA in the Patriot Hills BIA. To analyse the DNA content of the ancient ice across the Patriot Hills profile, a new protocol for extracting

DNA from large (~5–7 l) discrete ice core samples was devised (Supplementary Information). The novel ability to process very large-volume samples of ancient Antarctic ice in the field (that is, ~7 kg per temporal sample) under sealed sterile conditions creates a powerful new opportunity to generate sufficient concentration to permit detailed genetic biodiversity surveys. Samples were extracted across the profile to extract 16S rRNA for analysis at 7.5, 13.7, 16.0, 24 and 35 kyr BP to compare taxa across the profile to better understand the diversity of the biomarkers captured in the record. While a limited sample set, the samples covered the full range of glacial to interglacial conditions from the profile, and crucially the LGT (Fig. 4).

Strict ancient DNA methodologies designed to assess low-biomass microbial samples were applied at all times. Within the Australian Centre for Ancient DNA (ACAD), all work was conducted within an ultraviolet-treated hood in a still-air room. Each 0.45 µm nitrocellulose filter was cut in half using a sterile scalpel blade. Using sterilized tweezers, one-half of the filter was extracted using the PowerLyzer soil DNA isolation kit (MOBIO), following the manufacturer's instructions, and the second was extracted using the cetyl trimethylammonium bromide (CTAB) method[61]. Both extraction methods were employed to examine microorganisms with different cellular wall structures. Extraction blank controls (EBCs), that is, extractions containing no sample, control samples from the field (for example, swabs of coring and filtering equipment) and blank filters were processed in parallel to monitor background DNA levels from laboratory reagents.

Following strict ancient DNA techniques[62], all DNA extracts and EBCs were amplified using published, universal bacterial 16S rRNA primers that are modified to include Illumina sequencing adapters and a unique sample-specific 12-bp Golay barcode[63]; forward primer 515F (AATGATACGGCGACCACCGAGATCTACACT-ATGGTAATTGTGTGCCAGCMGCCGCGGTAA) and barcoded reverse primer 806R (CAAGCAGAAGACGGCATACGAGATnnnnnnnnnnnnAGTCAGTCAGC CGGACTAC HVGTWTCTAAT). PCR amplifications of the 291 target region were performed in a 25 µl reaction mix containing 2.5 mM $MgCl_2$, 0.24 mM dNTPs, 0.24 µl of each primer, Invitrogen Platinum HiFi Taq polymerase in 10× reaction buffer (Applied Biosystems) and 2 µl DNA extract. The PCR protocol included the following parameters: 6 min at 95 °C, followed by 35 cycles of 95 °C for 30 s, 50 °C for 30 s and 72 °C for 30 s, and a final extension at 60 °C for 10 min. PCR amplifications were performed in triplicate and pooled to minimize PCR bias, and a no-template PCR amplification control was included to monitor background DNA levels in PCR reagents. Pooled PCR products were purified using an Agencourt AMPure XP PCR purification kit (Beckman Coulter Genomics), and quantified using the HS dsDNA Qubit assay on a Qubit 2.0 fluorometer (Life Technologies). Purified PCR products from all samples were pooled at equimolar concentrations, and diluted to 2 nM for sequencing using a 300 cycle, 2 × 150 bp Illumina MiSeq kit.

Following DNA sequencing, all individually indexed 16S rRNA libraries were de-multiplexed from raw bcl files using CASAVA version 1.8.2 (Illumina), allowing for one mismatch. Sequencing adapters were removed from reads using Cutadapt v.1.1, and sequences were quality filtered (that is, reads >100 bp and >Q20 for 90% of each sequence) using the fastx toolkit v.0.0.14 (https://github.com/agordon/fastx_toolkit.git). Processed sequences were then formatted for use with QIIME v.1.8.0[64], and sequences with greater than 97% similarity to the Geengenes v13 reference database[65] were binned into operational taxonomic units (OTUs) using closed reference clustering in UCLUST. Representative sequences of each OTU were chosen by selecting the most abundant sequence from collapsed sequences. To assess the levels of contamination from laboratory reagents, OTUs detected in the EBCs, known laboratory contaminants[66] and genera identified in the Human Oral Microbiome Database (HOMD)[67] were filtered from the experimental samples. After filtering, an average of 1.417 sequences per sample remained (minimum of 4 and maximum of 7,174 sequences per sample). Extraction methods for each location were pooled, and alpha diversity (diversity within the sample) was compared using Simpson's, Chao 1, and observed species indexes in QIIME with the following parameters (minimum 20, maximum 200; step 10); no statistically significant differences in diversity were detected. Specific taxa were summarized by collapsing OTUs at genus level (Fig. 4). Marine taxa were identified by comparisons to Tara Oceans[68], or by performing literature searches for the 'taxon name; marine' and determining whether a marine source for the taxon was present within the first ten publications (Supplementary Information).

Data availability

The data supporting this study is available at National Oceanic and Atmospheric Administration Paleoclimatology Database (https://www.ncdc.noaa.gov/paleo/study/29415). The data from core MD07-3134 are available on the PANGEA Database at https://doi.pangaea.de/10.1594/PANGAEA.819646 and https://doi.pangaea.de/10.1594/PANGAEA.789348. Source data for Figs. 1, 4 and 5 and Extended Data Fig. 1 are available with the paper.

References

56. Iannone, R. Splitr: Use the HYSPLIT model from inside R. R package version 0.4.0.9000 https://www.rdocumentation.org/packages/SplitR/versions/0.4 (2019).
57. Carslaw, D. C. & Ropkins, K. Openair—an R package for air quality data analysis. *Environ. Model. Softw.* **27–28**, 52–61 (2012).
58. Reijmer, C. H., Greuell, W. & Oerlemans, J. The annual cycle of meteorological variables and the surface energy balance on Berkner Island, Antarctica. *Ann. Glaciol.* **29**, 49–54 (1999).
59. Abram, N. J., Mulvaney, R., Wolff, E. W. & Mudelsee, M. Ice core records as sea ice proxies: an evaluation from the Weddell Sea region of Antarctica. *J. Geophys. Res.* **112**, D15101 (2007).
60. Fox, B., Thorn, R., Anesio, A. & Reynolds, D. M. The in situ bacterial production of fluorescent organic matter; an investigation at a species level. *Water Res.* **125**, 350–359 (2017).
61. Tuner, C. R., Miller, D. J., Coyne, K. J. & Corush, J. Improved methods for capture, extraction, and quantitative assay of environmental DNA from Asian bigheaded carp (*Hypophthalmichthys* spp.). *PLoS ONE* **9**, e114329 (2014).
62. Adler, C. J. et al. Sequencing ancient calcified dental plaque shows changes in oral microbiota with dietary shifts of the Neolithic and Industrial revolutions. *Nat. Genet.* **45**, 450–455 (2013).
63. Caporaso, J. G. Ultra-high-throughput microbial community analysis on the Illumina HiSeq and MiSeq platforms. *ISME J.* **6**, 1621–1624 (2012).
64. Caporaso, J. G. QIIME allows analysis of high-throughput community sequencing data. *Nat. Methods* **7**, 335–336 (2010).
65. DeSantis, T. Z. et al. Greengenes, a chimera-checked 16S rRNA gene database and workbench compatible with ARB. *Appl. Environ. Microbiol.* **72**, 5069–5072 (2006).
66. Salter, S. J. et al. Reagent and laboratory contamination can critically impact sequence-based microbiome analyses. *BMC Biol.* **12**, 87 (2014).
67. Chen, T. et al. The Human Oral Microbiome Database: a web accessible resource for investigating oral microbe taxonomic and genomic information. *Database* **2010**, baq013 (2010).
68. Sunagawa, S. et al. Structure and function of the global ocean microbiome. *Science* **348**, 1261359 (2015).

Acknowledgements

C.J.F., C.S.M.T., L.M., N.R.G., L.S.W. and A.C. are supported by their respective Australian Research Council (ARC) and Royal Society of NZ fellowships, and C.J.F. and A.G.C. thank Keele University for a Research Development Award that underpinned this research at Keele University IceLab and Exeter University. Fieldwork was undertaken under ARC Linkage Project (LP120200724), supported by Linkage Partner Antarctic Logistics and Expeditions, whose enduring support we acknowledge. CSIRO's contribution was supported in part by the Australian Climate Change Science Program (ACCSP), an Australian Government Initiative. S.D. acknowledges financial support from Coleg Cymraeg Cenedlaethol and the European Research Council (ERC grant agreement no. 25923). M.E.W. acknowledges support from the Deutsche Forschungsgemeinschaft (grant no. We2039/8-1). Finally, we thank H. Glanville for comments on the final draft of the manuscript, and A. Jeffery for advice on SEM analysis.

Author contributions

C.J.F., C.S.M.T., A.B. and A.C. conceived this research. C.J.F., C.S.M.T., A.B., M.E.W., D.E., M.R., D.P.T., T.D.vO., A.D.M., M.A.J.C., S.D., M.I.B., N.C.M., J.V., A.R., L.M., H.M., CM, J.Y., M.M., A.G.C., M.R.P.H., A.P., J.L. and L.S.W. undertook analysis and sampling. C.J.F., C.S.M.T., A.B., M.E.W., M.R.P.H. and A.C. wrote the manuscript with input from all the authors.

Competing interests

The authors declare no competing interests.

Additional information

Extended data is available for this paper at https://doi.org/10.1038/s41561-020-0587-0.

Supplementary information is available for this paper at https://doi.org/10.1038/s41561-020-0587-0.

Correspondence and requests for materials should be addressed to C.J.F.

Peer review information Primary Handling Editor: James Super.

Reprints and permissions information is available at www.nature.com/reprints.

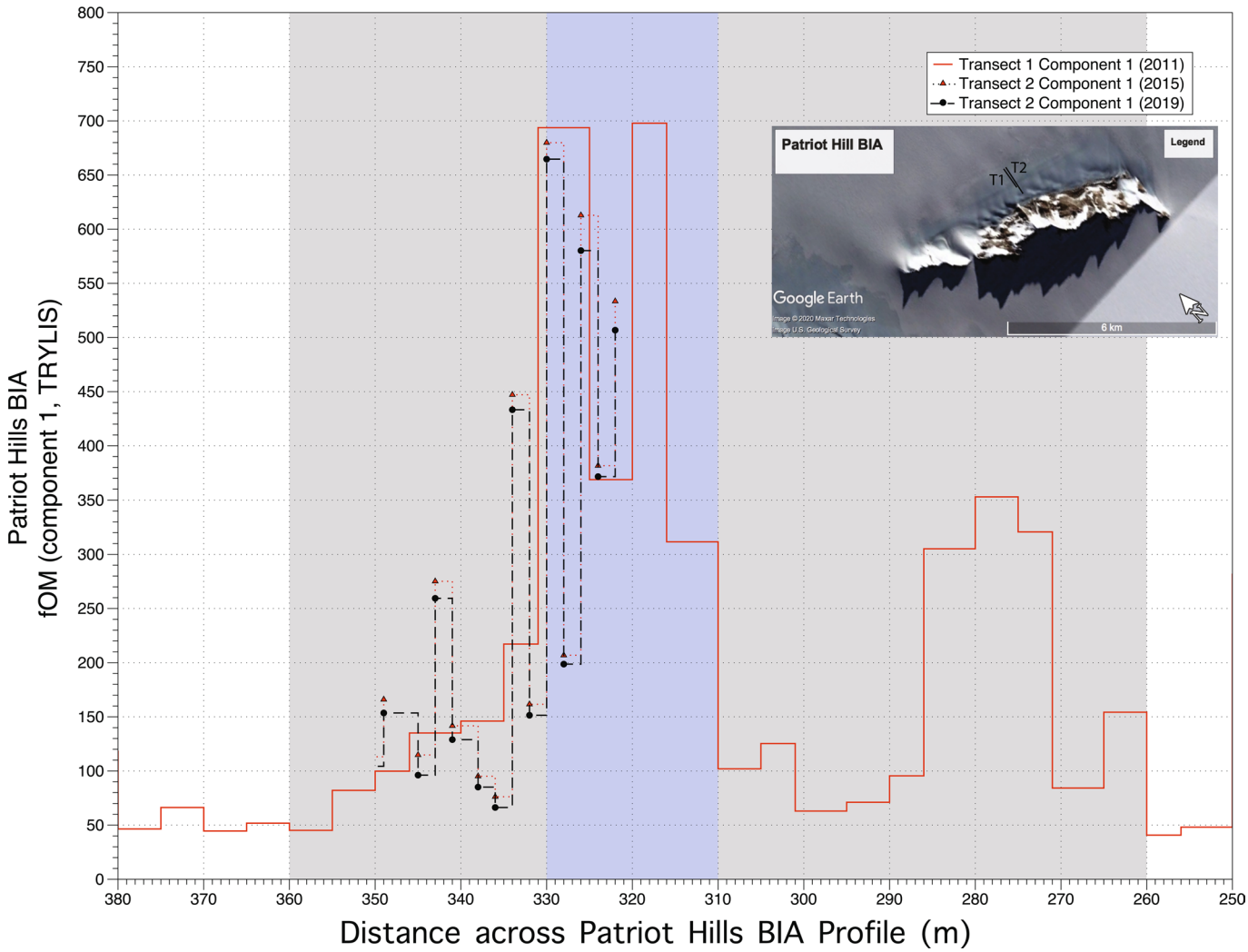

Extended Data Fig. 1 | Reproducibility of fOM signal. Reproducibility of fOM signal. 5 m resolved fOM concentration (Component 1; TRYLIS in red), plotted against data from a second parallel transect from the Patriot Hills transect (~3 m resolved black dashed line). The dashed lines represent replicate samples from the same transect which were taken in 2014/15 and measured in 2015 at UNSW Icelab (black dots), and subsequently reanalysed in 2019 at Keele Icelab (red triangles). The records are synchronised from water stable isotopes, site survey data and DGPS, and taken within 4 m of one another from a parallel transect (inset).